

## Phase Coexistence in Clusters

Charles L. Cleveland, Uzi Landman,\* and W. D. Luedtke

School of Physics, Georgia Institute of Technology, Atlanta, Georgia 30332

Received: April 5, 1994\*

An analytical cluster wetting model is developed, based on minimization of an expression for the free energy, for solid–liquid equilibrium coexistence states in clusters. For given materials' characteristic interfacial energies of the solid and liquid phases, the model relates the fraction of the solid-phase area wetted by the liquid to the volume fraction of the two phases. Equilibrium coexistence states with nonwetting, partial wetting, and complete wetting geometries, and their dependence on materials' properties and conditions of the system, are investigated. Analyses of molecular dynamics simulations of equilibrium solid–liquid coexistence in  $(\text{NaCl})_{1000}$  and  $\text{Ni}_{1289}$  clusters illustrate the higher self-wetting propensity of metals than that of ionic salts, and the results are in correspondence with the predictions of our model and experimental data.

### I. Introduction

The existence and properties of equilibrium phase coexistence in finite systems are subjects of current interest.<sup>1–13</sup> At the small cluster size regime molecular dynamics (MD) simulations led to the suggestion<sup>1,2b</sup> that the very notion of thermodynamic equilibrium coexistence between solid and liquid phases should be generalized for such systems to include “dynamic coexistence” where for given conditions (number of particles, temperature, pressure) an ensemble of such clusters may fluctuate between states which at any instant can be characterized as composed of clusters which are entirely solid or entirely liquid. Furthermore, it was shown via MD simulations<sup>4</sup> of sodium clusters,  $(\text{NaCl})_n$ , of variable size that while such “dynamic coexistence” occurs for small clusters, in larger ones ( $n \sim 100$ ) “conventional” equilibrium coexistence is established between solid and liquid phases in contact with one another in the same cluster (that is, during long-time MD simulations part of the cluster is liquid and part solid at all times). In these simulations it was also found that at coexistence the liquid part of a sodium chloride cluster, composed of 108 NaCl molecules, did not surround the solid portion,<sup>4</sup> forming instead a droplet adsorbed on one of the (100) faces of the solid phase, while at coexistence a silicon cluster (containing 1024 atoms) consisted of a solid crystalline inclusion surrounded (wetted) almost completely by a molten liquid shell.<sup>5</sup> These early observations led to the formulation of a model which correlated the coexistence topology in clusters with their self-wetting propensity.<sup>5</sup> Accordingly, for self-wetting materials (such as argon, metals, and to a large degree silicon) a coexistence topology of a liquid surrounding a solid crystalline inclusion is expected, while for non-self-wetting materials (such as alkali halides) a phase coexistence topology corresponding to a solid portion forming only partial contact with the liquid phase is predicted.

In section II we develop a new model which, for given characteristic materials parameters (interfacial energies) and relative volume fractions of the solid and liquid phases, allows, under certain model assumptions, prediction of the equilibrium coexistence topology and geometry of the cluster. Details of the molecular dynamics simulations and methods of analysis are given in section III. In section IV we present results of MD simulations for clusters of sodium chloride and nickel and discuss them in the context of our “cluster wetting model” (CWM).

### II. Cluster Wetting Model

Consider a finite but macroscopic cluster containing  $N$  atoms, and of fixed volume  $\Omega$ , i.e., one which is sufficiently large to support equilibrium coexistence between liquid and solid phases (for simplicity we consider a one-component system. Treatment of a multicomponent system is straightforward). Under conditions of a fixed temperature,  $T$ , and chemical potential (or equivalently pressure),  $\mu = \mu_0(T)$  (where  $\mu_0$  denotes the value at coexistence), which for a macroscopic cluster are consistent with bulk coexistence of a solid and a liquid phase, the  $N$  particles of the system will arrange in a configuration where part of the system, containing  $n_s = \rho_s(T)\Omega_s$  particles, is solid (where  $\rho_s$  and  $\Omega_s$  are the solid density and volume, respectively) and part liquid, containing  $n_l = \rho_l(T)\Omega_l$  particles ( $\rho_l$  and  $\Omega_l = \Omega - \Omega_s$  are the liquid density and volume, respectively), such that

$$N = n_s(T) + n_l(T) \quad (1)$$

Under these conditions the free energy of the system contains bulk and interfacial contributions<sup>7</sup>

$$F(N, \Omega, T) = f_s(\rho_s, T)\Omega_s + f_l(\rho_l, T)(\Omega - \Omega_s) + F_i^{sv}(T; \Omega_s) + F_i^{sl}(T; \Omega_l) + F_i^{sl}(T; \Omega_s, \Omega_l) \quad (2)$$

where  $f_s$  and  $f_l$  are the bulk free energies per unit volume of the coexisting uniform solid and liquid phases,  $F_i^{ab}$  are the contributions from the inhomogeneous interfacial regions separating the bulk phases,  $F_i^{sl}$  is the interfacial free energy between the solid and liquid phases, and  $F_i^{sv}$  and  $F_i^{sl}$  are the solid–vapor and liquid–vapor interfacial energies. The interfacial free energies depend on the interfacial surface areas. In this context we remark that in statistical mechanics the definitions of  $\Omega_s$  and the interfacial areas between phases customarily follow the Gibbs convention, where the excess volume and number associated with an interface are taken to be zero.<sup>7,14,15</sup> This choice is made since the interfacial region is “diffuse”, lacking a sharp microscopic definition (see also section III.B).

The interfacial terms in the free energy correspond to contributions from the inhomogeneous regions separating the homogeneous bulk phases and are the ones which are sensitive to the shape of the crystalline (solid) component and curvature of the liquid (the latter one introduces “ $1/R$  effects”, where  $R$

\* Abstract published in *Advance ACS Abstracts*, June 1, 1994.

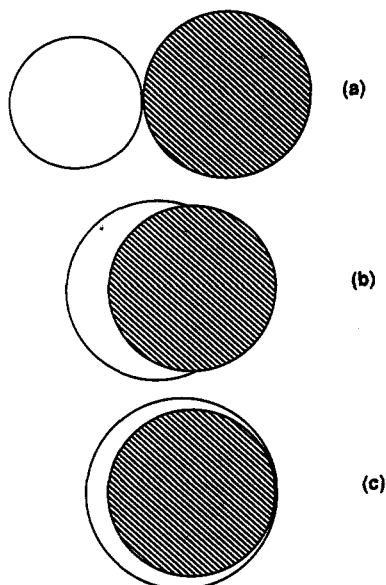


**Figure 1.** Schematics of phase coexistence topologies considered by our model. In the three cases shown the ratios of volumes of the liquid (blank) and solid (shaded) phases are the same. The top configuration represents a complete nonwetting case; the middle one corresponds to partial wetting (for the case shown the ratio of wetted surface of the solid to the total surface area of the solid is  $1/2$ ); the bottom configuration corresponds to the case of complete wetting of the solid phase.

is the mean curvature of the liquid, such as the Young–Laplace pressure difference and capillarity.<sup>16</sup> In general, the interfacial free energies involving the solid component ( $F_i^{sl}$  and  $F_i^{sv}$ ) are anisotropic, depending on the crystallography of the interphase interfaces (that is, the orientations of the crystalline faces, characterized by the surface normals  $\hat{m}$ ). Consequently, these interfacial free energies are expressed as<sup>7</sup>

$$F_i^{sl}(T; \Omega_s, \Omega_\ell) = \sum_{\hat{m}} \int_{S_{sl}(\hat{m})} dS'_{sl} f_i^{sl}(\hat{m}, T) \quad (3a)$$

and

$$F_i^{sv}(T; \Omega_s) = \sum_{\hat{m}} \int_{S_{sv}(\hat{m})} dS'_{sv} f_i^{sv}(\hat{m}, T) \quad (3b)$$

where  $f_i^{sl}(\hat{m}, T)$  and  $f_i^{sv}(\hat{m}, T)$  are the interfacial free energies per unit interfacial area of the corresponding interfaces, and the integrations are over the surface elements of these interfaces, relative to crystal axes. Minimization of eq 3a or 3b subject to the constraint of fixed volume  $\Omega_s$  was formulated and solved first by Wulff.<sup>17–19</sup> However, the constrained minimization problem posed by eqs 1–3 (supplemented by the constant total volume constraint) is a formidable problem and has been treated only in some special cases.<sup>6,7,9,10</sup>

In this study we focus on the topology of a finite cluster at solid–liquid coexistence. To gain insight into this problem, we wish to minimize the free energy (eq 2) for given fixed volumes of the cluster and of the solid and liquid phases, under certain simplifying assumptions which we specify below.

We model our cluster as a spherical solid portion of fixed volume,  $\Omega_s$ , and density,  $\rho_s$ , in contact with a liquid of fixed volume  $\Omega_\ell$  and density  $\rho_\ell$ . The phase coexistence configurations which we consider include those where the solid sphere is fixed in shape while the liquid phase contacting the solid is allowed to assume the shapes of indented spherical figures, ranging from two spheres touching at a point to a solid spherical inclusion surrounded by a liquid shell (see Figure 1).

By limiting ourselves to these coexistence configurations, we do not include contributions due to crystallographic anisotropies of interfacial free energies of the solid, changes in the shape of the solid phase, formation of a capillary meniscus localized at the

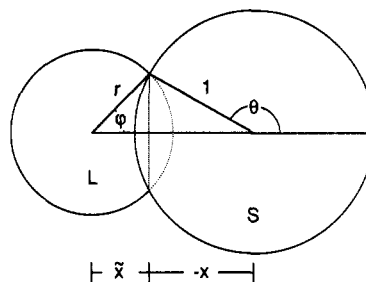


**Figure 2.** Schematic of phase coexistence geometry with the liquid phase described by the indented spherical figure (L) of radius  $r$ , and the solid phase described by the solid sphere (S) of unit radius. The definitions of angles and distances used in the text are included.

periphery of the contact zone between the liquid and the solid (the length scale associated with the meniscus is taken to be smaller than all other relevant lengths in the system), and curvature corrections to the interfacial free energy of the liquid. With these assumptions our model is certainly not a substitute for more complete ones, particularly those which maintain the crystallographic anisotropies.<sup>9,10</sup> Rather, it is intended to provide an analytically soluble model, against which our simulation results (see section IV) may be readily compared. (We note that our model is certainly applicable for cluster coexistence of two immiscible fluid phases, coexisting with and embedded in a third, where the lack of anisotropy and assumed local spherical shapes of the interfaces are justified. Generalization of our model in this case to include three interfaces with different radii of curvature is possible.) In this context we remark that while it is possible to solve numerically the constrained minimization problem posed in eqs 1–3, with the crystalline anisotropies maintained,<sup>10</sup> large sensitivity of the results to input data which in most cases is not available (such as crystallographic dependence of interfacial free energies, and the variations of interfacial free energies with temperature) often introduces significant uncertainties in quantitative analyses of specific materials.<sup>10</sup> We also note, a posteriori, the satisfactory correspondence between the predictions of our model and the results of our molecular dynamics simulations (see section IV).

In order to obtain the expression for the free energy of the system, and the condition for the optimal solid/liquid coexistence geometry, it is convenient to take the radius of the solid sphere as the unit of length. With this unit of length of distances  $X$  and  $\tilde{X}$  indicated in Figure 2 are given by  $X = \cos \theta$  and  $\tilde{X} = r \cos \phi$  where the reduced radius of the liquid spherical figure is given by  $r^2 = \tilde{X}^2 - X^2 + 1$ . In terms of these quantities the expressions for the various volumes and interfacial areas which enter the expression for the free energy may be written as follows:

$$\Omega_s = \frac{4\pi}{3} \quad (4a)$$

$$\Omega_\ell = \frac{\pi}{3} (2r^3 + 3r^2 \tilde{X} - \tilde{X}^3) - \frac{\pi}{3} (2 + 3X - X^3) \quad (4b)$$

$$S_{\ell v} = 2\pi(r^2 + r\tilde{X}) \quad (4c)$$

$$S_{sv} = 2\pi(1 - X) \quad (4d)$$

$$S_{sl} = 2\pi(1 + X) \quad (4e)$$

where  $\Omega_s$  and  $\Omega_\ell$  are the volumes of the solid and the liquid phases (and the total volume of the cluster is  $\Omega = \Omega_s + \Omega_\ell$ ) and  $S_{\ell v}$ ,  $S_{sv}$ , and  $S_{sl}$  are the interfacial surface areas of the liquid/vapor, solid/vapor, and solid/liquid interfaces, respectively. Denoting the corresponding interfacial free energies (per unit area) by  $\sigma_{\ell v}$ ,  $\sigma_{sv}$ , and  $\sigma_{sl}$  (which are temperature dependent) allows the free energy of the cluster (eq 2) to be written as

$$\begin{aligned}
 F(T, \Omega) / 4\pi &= F_{\Omega}(T, \Omega_{\ell}, \Omega_s) + \sigma_{\ell v} S_{\ell v} + \sigma_{sv} S_{sv} + \sigma_{s\ell} S_{s\ell} \\
 &= F_{\Omega}(T, \Omega_{\ell}, \Omega_s) + \frac{1}{2} \sigma_{\ell v} (r^2 + r\bar{X}) + \\
 &\quad \frac{1}{2} \sigma_{sv} (1 - X) + \frac{1}{2} \sigma_{s\ell} (1 + X) \quad (5)
 \end{aligned}$$

where  $F_{\Omega}$  is the total volume free energy of the system which is independent of the geometry of the cluster.

The coexistence geometry which minimizes the free energy of the cluster can be characterized by the value of  $X$  which is the solution to the equation  $dF/dX = 0$ , subject to the constant volume constraints, yielding

$$\begin{aligned}
 \Sigma \equiv \frac{\sigma_{sv} - \sigma_{s\ell}}{\sigma_{\ell v}} = \\
 \left( 2\bar{X} + r + \frac{\bar{X}^2}{r} \right) \left( \frac{6rX + 6X\bar{X} + 3 - 3X^2}{6r\bar{X} + 6\bar{X} + 3 - 3X^2} \right) - \frac{X\bar{X}}{r} - 2X \quad (6)
 \end{aligned}$$

It can also be shown that for  $-1 < \Sigma < 1$  the second derivative of the free energy is positive and that in fact the solution to eq 6 gives the global minimum of the free energy, and thus the equilibrium coexistence configuration. Clusters with  $\Sigma \leq -1$  are completely unwetted, while those with  $\Sigma \geq 1$  are completely wetted.

Consider now a particular coexistence state of the cluster with a volume fraction  $\Gamma = \Omega_{\ell}/\Omega_s$  between the liquid and solid phases (considering an isolated cluster, different values of  $\Omega_{\ell}$  and  $\Omega_s$  and thus  $\Gamma$  can be accessed by varying the total energy of the cluster; this, microcanonical, route is the one which we used in our MD simulations, described in sections III and IV). Using eqs 4a,b we establish a relationship between  $X$  and  $\bar{X}$  (since  $r$  in eq 4b is a function of these two variables). Therefore we may express the free energy and the rhs of eq 6 as functions of  $X$  and  $\Gamma$ . It is natural to inquire what fraction of the surface of the solid phase is covered by the liquid for a given value of  $\Gamma$ . Denoting this fraction by  $\zeta = S_{s\ell}/4\pi$ , we obtain from eq 4e the relation  $\zeta = (1 + X)/2$ , which varies between  $\zeta = 0$ , corresponding to a configuration of a solid sphere touching at a point a spherical liquid droplet, and  $\zeta = 1$ , corresponding to a spherical solid inclusion completely surrounded by a liquid shell. Intermediate values of  $\zeta$  correspond to coexistence configurations with variable degrees of coverage of the surface of the solid phase by the liquid.

We may now express the equilibrium geometry condition (eq 6) in terms of  $\zeta$  and  $\Gamma$  as

$$\frac{\sigma_{sv} - \sigma_{s\ell}}{\sigma_{\ell v}} = H(\zeta, \Gamma) \quad (7a)$$

where the function  $H$  represents the right-hand side of eq 6 expressed in terms of  $\zeta$  and  $\Gamma$ . This function obeys  $-1 \leq H(\zeta, \Gamma) \leq 1$  for all values of  $\Gamma$ , with  $H(0, \Gamma) = -1$  and  $H(1, \Gamma) = 1$ . It is interesting to note that eq 7a written in the form

$$\sigma_{sv} - \sigma_{s\ell} - H(\zeta, \Gamma) \sigma_{\ell v} = 0 \quad (7b)$$

may be regarded as a generalization of the spreading coefficient (or wetting condition) for a liquid in coexistence with a planar surface,<sup>20</sup>  $\mathcal{L} = \sigma_{sv} - \sigma_{s\ell} - \sigma_{\ell v}$ , where for negative  $\mathcal{L}$  the surface in contact with the liquid prefers to remain dry, and  $\mathcal{L} > 0$  corresponds to wetting of the surface (the value  $\mathcal{L} = 0$  marks the onset of complete wetting). Similarly, when  $\zeta = 1$ , corresponding to complete wetting of the solid spherical inclusion by a liquid shell,  $H(\zeta, \Gamma) = 1$  and eq 7b coincides with the planar surface wetting condition ( $\mathcal{L} = 0$ ).

We may now evaluate, for given materials' interfacial energies (left-hand side of eq 7a) and liquid to solid volume fraction  $\Gamma$ ,

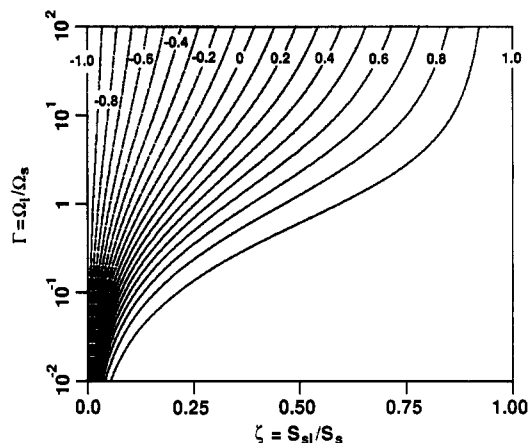


**Figure 3.** Contours of  $\Gamma = \Omega_{\ell}/\Omega_s$  versus  $\zeta = S_{sl}/S_s$  for different values of the material-dependent parameter  $\Sigma \equiv (\sigma_{sv} - \sigma_{s\ell})/\sigma_{\ell v}$  (see eq 7a). A logarithmic scale is used for  $\Gamma$ . Note that for  $\Sigma \geq 1$ ,  $\zeta = 1$ , corresponding to a solid inclusion wetted completely by the liquid phase.

the corresponding value of  $\zeta$  which characterizes the equilibrium phase coexistence geometry (see Figure 3).

The main trends predicted by our model, pertaining to the topology and geometry of solid/liquid coexistence in cluster, are exhibited in where equilibrium values of  $\zeta$  (fraction of wetted surface of the solid phase) are plotted versus  $\Gamma$  (volume fraction between the coexisting liquid and solid phases), for different choices of the material's specific parameter  $\Sigma \equiv (\sigma_{sv} - \sigma_{s\ell})/\sigma_{\ell v}$ . These include the following:

(i) For a given value of  $\Sigma$ , the fraction of the wetted surface of the solid phase,  $\zeta$ , increases upon increasing  $\Gamma$ , corresponding to increased wetting of the solid phase by the liquid.

(ii) For a given liquid/solid volume fraction  $\Gamma$ , enhanced wetting occurs for larger values of  $\Sigma$ . For materials with  $\Sigma \leq 0$ , the larger fraction of the solid surface remains unwetted even for relatively large values of  $\Gamma$ . For small values of  $\Gamma$ , the larger part of the solid surface remains unwetted even for large values of  $\Sigma < 1$ . Even for  $\Gamma \gtrsim 1$  and large  $\Sigma$  (that is, materials with pronounced wetting propensity), as long as  $\Sigma < 1$ , the solid phase remains partially unwetted, exposing a solid/vapor interface. We term such singly connected coexistence topologies as "lensing topologies".<sup>21</sup>

(iii) For  $\Sigma = 1$  the coexistence topology of the cluster is predicted to be not singly connected, consisting of a solid inclusion surrounded by a liquid shell (complete wetting), for all volume fractions  $\Gamma$ .

### III. Molecular Dynamics Simulations and Analysis

**A. Molecular Dynamics Simulations.** Having presented in the previous section our model and consequences thereof pertaining to interphase coexistence geometries in clusters, we turn now to MD simulations of solid/liquid coexistence in clusters. To illustrate various coexistence topologies and their dependence on material-specific energetic parameters (interfacial energies), we chose for our simulations two materials systems (a metal and an ionic material) which differ in their nature of bonding, cohesion, and interatomic (or interionic) interactions.

In metals the contributions to the cohesive energy are associated with the energetic properties of the delocalized electron gas, the embedding energy of metal ions in the electronic charge distribution, and the interactions between screened ion cores. In our simulations of coexistence in a nickel cluster containing 1289 atoms ( $\text{Ni}_{1289}$ ) we have used many-body interactions obtained via the embedded-atom method (EAM).<sup>22</sup> We have previously used these interactions in studies of nickel clusters<sup>19</sup> as well as investigations of the solid-liquid interface and surface melting of nickel.<sup>23</sup>

In ionic material (such as alkali halides), bonding is electrostatic in nature. To model the interphase properties of a  $(\text{NaCl})_{1000}$  cluster, we have used the interionic interactions proposed by Macrold et al.,<sup>24</sup> which contain direct Coulomb point charge interactions, Born–Mayer repulsions, and dispersion contributions.

In all our simulations we started from a solid crystalline cluster and, using the appropriate interaction potentials, the Newtonian equations of motion were integrated using the Gear fifth-order predictor-corrector algorithm<sup>25</sup> with an integration time step of 0.5 fs. The energy content of the cluster can be controlled via scaling of particle velocities. For finite-size systems, coexistence configurations with various degrees of melting of the cluster (i.e., differing coexistence liquid/solid ratios,  $\Gamma$ ) are accessible. Consequently, to isolate a particular value of  $\Gamma$ , our simulations are performed in the microcanonical ensemble; that is, subsequent to the total energy of the system being brought to a desired value, via uniform scaling of the particle velocities, the system evolves dynamically with no further thermalization, establishing a coexistence state characterized by a value of  $\Gamma$ , an average temperature  $T$ , and an interphase coexistence topology.

**B. Analysis of the Simulations.** In order to examine molecular dynamics simulations of cluster wetting in light of the theoretical model described in section II, we must first be able to distinguish between atoms in solid regions of a simulated cluster and those in liquid regions. We also need to be able to calculate the volumes the two phases occupy, as well as surface areas for the solid–vacuum and solid–liquid interfaces. None of these quantities can be determined without some ambiguity.

Consider the difficulty of dividing the system up into “liquid” and “solid” atoms. Interphase interfaces are inhomogeneous in nature, and the transition region connecting the two phases is of narrow spatial extent in comparison to the dimensions of the interfacing bulk phases. Structural, energetic, and transport properties in the interfacial regions are inhomogeneous and nonisotropic.<sup>15,23,26–31</sup> Examining local atomic structure within the cluster is in general not discriminating enough to distinguish liquid atoms from disordered solid ones. Also, examining a property such as atomic potential energy might work for some systems and not for others. It has the disadvantage that it effectively averages over a volume of the system equal to the range of the potential. Consequently, we propose that to distinguish “liquid” from “solid” particles, it may be better to examine the simulation for some time span and use the expectation that liquid atoms will move farther than solid ones. Proceeding along this line, we calculate  $\sigma$ , the standard deviation of the position of each atom within some time interval divided by the square root of the length of the time interval.<sup>32</sup> This method has its own problems, however: If the time span is too short, the behaviors of atoms in the liquid and solid are too similar to clearly distinguish between them, and if the span is too long, many atoms will have changed phases, resulting in a value for  $\sigma$  that is an average between liquid and solid behaviors, obscuring the distinction between solid and liquid atoms. Fortunately, there is a rather large range of time intervals for which  $\sigma$  is relatively insensitive (we have used a time interval of about 50 ps for all the systems we report here).

Let us suppose we have accepted  $\sigma$ , calculated over some time span, as being a suitable measure of “solidity” or “liquidity”. We still face a more fundamental problem if we want to look at small clusters, which would persist even if we choose any different criterion for identifying the macroscopic phases in our model. In systems large enough, one can properly speak of systems as being composed of solid, liquid, and gaseous regions, with the interfaces between them having negligible volume. Certainly our model takes this sort of approach. When systems of a few thousand atoms are considered, however, the interfacial volume, while negligible in the macroscopic view, becomes a substantial fraction of the whole. If we insist on dividing such a small cluster strictly

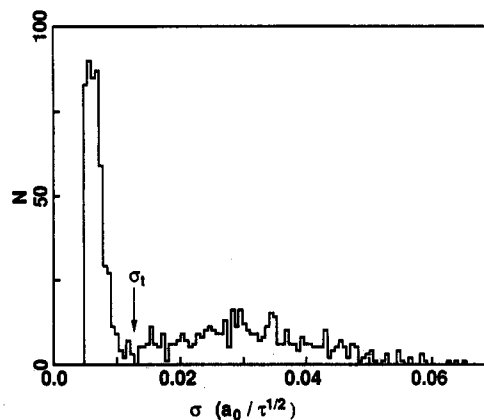


**Figure 4.** Histogram of the number of particles versus the root-mean-square displacement of the atom, divided by the square root of the time interval (abscissa in units of  $a_0/\sqrt{\tau}$ , where  $a_0$  is the Bohr radius and  $\tau = 1.033$  fs).  $\sigma_t$  denotes the value used to distinguish solid ( $\sigma < \sigma_t$ ) from liquid ( $\sigma > \sigma_t$ ) particles. The histogram corresponds to the case of a  $(\text{NaCl})_{1000}$  cluster at an average temperature  $T = 950$  K (see Table 1 and Figure 5a).

between “solid” and “liquid” parts, we cannot expect an utterly clear discrimination between the phases to be possible, since a significant fraction of the atoms in a small cluster will have interfacial properties instead of bulk ones.

This difficulty can be seen in Figure 4, which shows a histogram of number of particles vs  $\sigma$  for the case of  $(\text{NaCl})_{1000}$  cluster. The value of  $\sigma$  chosen to distinguish between solid and liquid atoms, which we call  $\sigma_t$ , is necessarily arbitrary to some degree, since atomic properties vary almost continuously within a small cluster because of its essential inhomogeneity. Fortunately, the precise value chosen for  $\sigma_t$  turns out not to be critical. Perhaps this indicates that clusters of around 1000 atoms are sufficiently large to permit cautious macroscopic modeling. Our previous studies of the energetics of small, cold metallic clusters also supports this view.<sup>19</sup> For the case shown in Figure 4, all atoms with  $\sigma < \sigma_t$  are considered as belonging to the solid phase and those with  $\sigma > \sigma_t$  to the liquid phase.

Given that we have classified all the atoms as either liquid or solid, we can turn to the determination of volumes and surface areas. The calculations of areas will inevitably require us to identify atoms that are on or at various interfaces of the cluster, a necessarily vague classification in light of the previous discussion. Because of this vagueness, we would like to use a method which has very few adjustable parameters. In light of the model, we want it to return volume and surface areas directly and allow identification of the different types of interfaces in a natural way. As a last measure of reasonableness, we want a method which can locate the interfaces sensibly when visually compared with images such as those in Figures 5 and 6 (the histogram in Figure 4 corresponds to Figure 5a). Of various approaches we have tried, the most successful one is a modification of three-dimensional Delaunay triangulation.

Normally, Delaunay triangulation has no adjustable parameters. It subdivides a volume containing an arbitrary set of points into nonoverlapping and space-filling tetrahedra, whose vertices fall at the points. This decomposition is unique if no sphere can be constructed on which more than four vertices lie. A substantial number of algorithms are to be found in the literature,<sup>33</sup> and at least one efficient implementation is available in Fortran as part of GEOMPACK.<sup>34</sup>

We begin by performing such an ordinary Delaunay triangulation, where the points are the atomic positions. Let us call any tetrahedron all of whose atoms are solid, in the sense described above, a “solid” tetrahedron and call any other tetrahedron “wet”. We take the volume of the solid part of the cluster to be the sum of the volumes of the solid tetrahedra, and the volume of the liquid to the sum of the volumes of the rest. If a face is shared

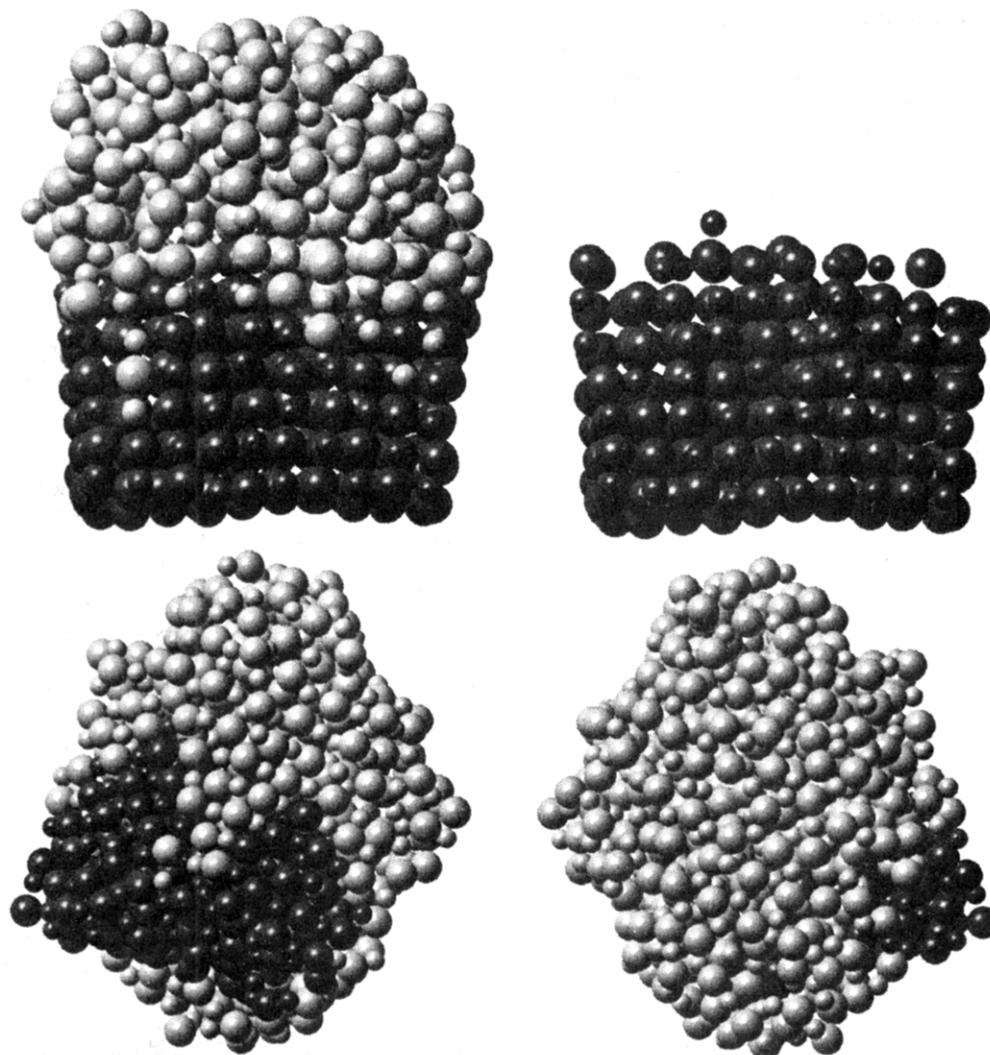


**Figure 5.** (a, Top) Side view of an atomic configuration obtained from a MD simulation of a  $(\text{NaCl})_{1000}$  cluster, corresponding to a solid-liquid equilibrium coexistence state with  $\Gamma = 1.06$  and  $\zeta = 0.46$  (see Table 1), illustrating the formation of a liquid droplet of molten salt wetting one of the faces of a solid crystal. Dark and light spheres correspond to solid and liquid ions with the larger spheres representing halide anions and the smaller ones sodium cations. The configuration on the right shows just the solid phase illustrating a, somewhat roughened, (100) interface. (b, Bottom) Same as part a for a  $(\text{NaCl})_{1000}$  cluster at an equilibrium coexistence state with a larger liquid to solid volume ratio ( $\Gamma = 3.97$ ) and  $\zeta = 0.64$ ; see Table 1. The left and right figures correspond to the same atomic configurations rotated by  $180^\circ$  (i.e., “front” and “back”). The atomic configuration illustrates the formation of solid lenses and faceting (mainly (100)) of the exposed (nonwetted) solid-vapor interfaces.

between a solid and a wet tetrahedron, we say that it is part of the solid-liquid interface. If a face on a solid tetrahedron is not shared by another tetrahedron, we take it as part of the solid-vacuum interface. If the face of a “wet” polyhedron is not shared, we say that it is part of the liquid-vacuum interface.

However, this procedure by itself does not always produce acceptable results: It often overestimates the liquid region. The reason is simply that Delaunay triangulation always fills out the convex hull of the set of points being triangulated, employing tetrahedra with arbitrarily long edges, if necessary. For example, if we had only one liquid atom sitting on the surface of a solid cluster, and we moved that atom farther and farther away from the cluster, according to the Delaunay construction alone the volume of the liquid would increase without bound and the fraction of the solid surface which was wet would increase until it was approximately half. This behavior is clearly not desirable.

Our modification involves introducing a length parameter,  $r_c$ . After making the usual Delaunay construction and classifying tetrahedra and faces as described above, we examine all the tetrahedral faces assigned to interfaces with the vacuum. If one has an edge which is longer than  $r_c$ , then its tetrahedron is eliminated. We repeat the steps of classification, examination, and elimination until no such “unsatisfactory” surface faces can

be found. With an appropriate value for  $R_c$ , this method seems to satisfy our criteria. Compare, for example, Figure 7, where we show the results of the tetrahedral decomposition for one of the NaCl clusters, with Figure 5a, where an atomic representation of the same system is shown. We refine our choices  $r_c$  by making such visual comparisons. For NaCl, we took  $r_c = 9.6a_0$ , which is about 90% of the crystal lattice constant. For Ni, we used a value of  $6.4a_0$ , which is just slightly larger than the second nearest neighbor distance. Further details of our method of analysis will be published elsewhere.

#### IV. Solid-Liquid Coexistence in Sodium Chloride and Nickel Clusters

Results of the MD simulations, analyzed as described in section III.B in light of the theoretical model presented in section II, are given in Figure 8 and Table 1 for the two systems considered by us. The corresponding atomic structures are shown in Figures 5 and 6.

The  $(\text{NaCl})_{1000}$  cluster is an example of a material characterized as partial-self-wetting, in the language of our model. As seen under conditions where  $\Gamma = \Omega_l/\Omega_s \approx 1$ , only less than half of the surface of the solid surface is wetted ( $\zeta = 0.46$ ), and the atomic configuration shown in Figure 5a shows that the liquid-solid

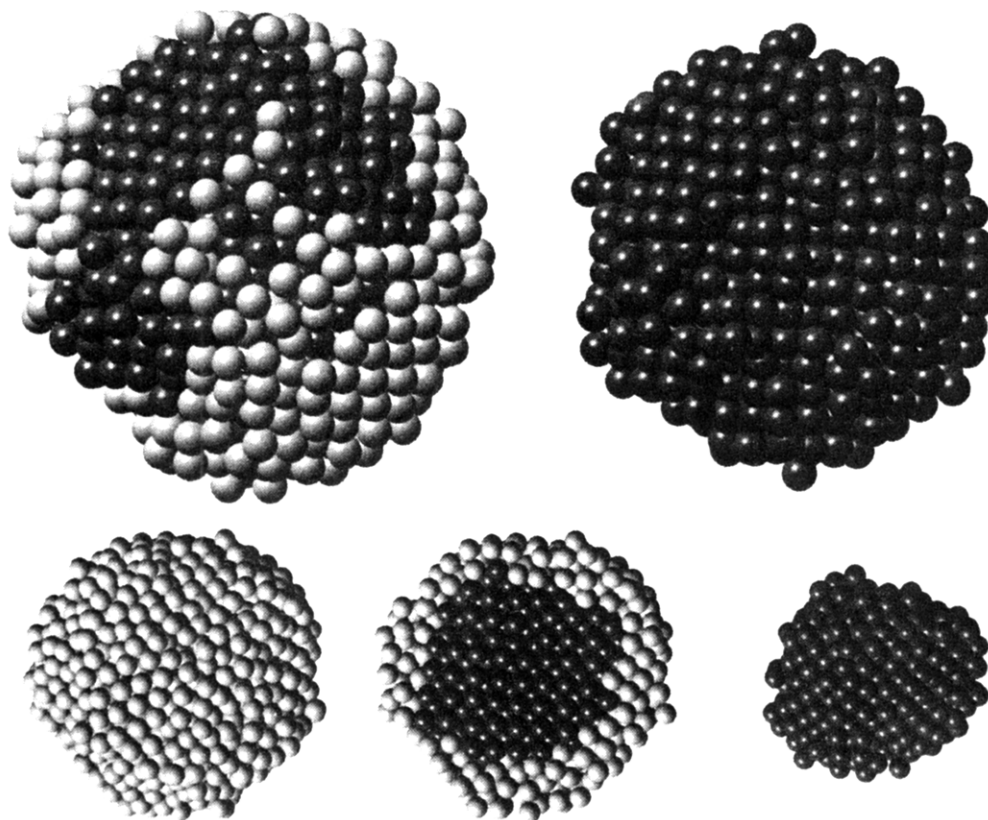


**Figure 6.** (a, Top) Atomic configuration obtained from a MD simulation of a  $\text{Ni}_{1289}$  cluster, corresponding to a solid–liquid equilibrium coexistence state characterized by  $\Gamma = 0.36$  and  $\zeta = 0.72$ . Solid and liquid atoms are represented by dark and light spheres, respectively. The figure on the left illustrates a wetted solid phase, exposing faceted (mainly (111)) solid lenses. The figure on the right shows just the solid phase, illustrating a faceted crystallite. The solid-to-liquid interface is established predominantly on (111) facets. (b, Bottom) Same as part a but for an equilibrium coexistence state of the nickel cluster characterized by  $\Gamma = 2.24$  and  $\zeta = 1$  (i.e., complete wetting of the solid phase). The figure in the middle shows a cut through the wetted cluster (left figure), illustrating a solid inclusion completely surrounded by the liquid. Shown on the right is just the solid inclusion.

**TABLE 1: Results for  $(\text{NaCl})_{1000}$  and  $\text{Ni}_{1289}$  Clusters at Different Solid–Liquid Coexistence States<sup>a</sup>**

	$\Gamma$	$\zeta$	$T$ (K)
NaCl	1.06	0.46	950
	3.97	0.64	940
Ni	0.36	0.72	1360
	2.24	1.00	1460

<sup>a</sup>  $\Gamma = \Omega_\ell/\Omega_s$  is the ratio between the volume of the liquid and solid phases, and  $\zeta = S_{\ell s}/S_s$  is the fraction of the surface of the solid phase wetted by the liquid. Both quantities were determined by the method described in section III.B. The average temperatures of the clusters are also given.

interface is localized on one face of the solid, with the liquid forming an “adsorbed” droplet. The solid exposes (100) surfaces, and the solid–liquid interface, which is also in the (100) direction, is somewhat “rough” on the atomic scale (a significant contribution to  $\zeta$  is due to the roughness of the solid–liquid interface). Furthermore, even for conditions of the system for which  $\Gamma \approx 4$ , only about two-thirds of the surface of the solid phase is wetted, with the unwetted solid facets appearing as “lenses” (see Figure 5b).

In contrast to the ionic cluster, the coexistence states of the metallic ( $\text{Ni}_{1289}$ ) cluster portray a behavior characteristic of materials with a high propensity for self-wetting. We observe that, even for a small value of  $\Gamma \approx 1/3$ , over two-thirds of the surface of the solid phase is wetted, with the liquid spreading over the surface as seen in Figure 6a (we note that for this value of  $\Gamma$  there are not enough liquid atoms to completely “coat” the solid part as a liquid monolayer). The incompletely wetted solid tends to expose (111) facet lenses. When  $\Gamma \sim 2.25$ , the solid phase is completely wetted ( $\zeta = 1$ ) by the liquid phase (see Figure 6b), with the solid–liquid interfaces mainly falling on (111) facets.

From Figure 8 we may deduce that, according to our cluster phase coexistence model, the value of the material-dependent parameter  $\Sigma (= (\sigma_{sv} - \sigma_{sl})/\sigma_{lv}$ ; see eq 6) for the ionic cluster is predicted to be  $\Sigma \approx 0.8$ , and that for the Ni cluster is  $\Sigma \geq 0.99$  or  $\Sigma \geq 1$  if we disregard the least melted Ni cluster ( $\Gamma = 0.36$ ; see Table 1), since there are not enough liquid atoms in it to completely wet the solid part of the cluster (see Figure 6a), regardless of  $\Sigma$ .

Experimental and theoretical values of the interfacial free energies for the materials studied here are rather uncertain, and furthermore, their dependence on temperature and surface crystalline orientation is in general not known. Nevertheless, calculations of  $\Sigma$  using published values for the interfacial energies<sup>35</sup> support our predictions.

## V. Summary

Equilibrium phase coexistence in clusters was investigated via an analytical model and molecular dynamics simulations. The cluster-wetting model (CWM), developed in section II, is based on minimization of an expression for the free energy of the cluster for given volumes of the solid and liquid phases and the assumptions of a spherical shape for the solid phase and indented spherical figures for the molten phase. The coexistence condition which we derived (eq 7) relates, for given values of (material dependent) interfacial energies, the volume ratio ( $\Gamma$ ) between the liquid and solid phases to the fraction of the surface of the solid phase which is wetted by the liquid ( $\zeta$ ). Thus, the CWM allows systematic investigations of the dependence of the geometry and topology of equilibrium coexistence states for a given material; that is, for a given value of  $\Sigma = (\sigma_{sv} - \sigma_{sl})/\sigma_{lv}$ , the dependence of  $\zeta$  on  $\Gamma$ , and consequently the geometries and topologies of the coexistence states, can be determined (the model allows variations

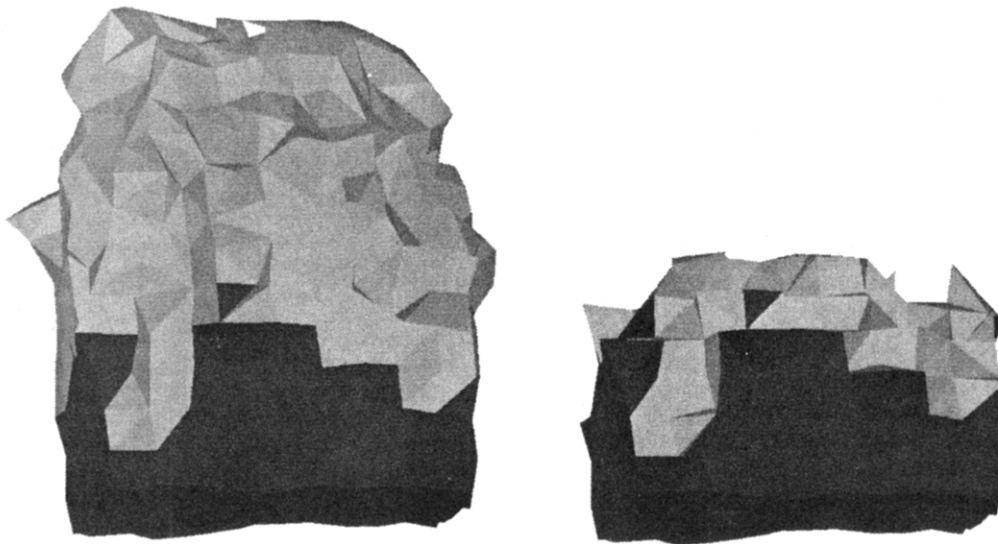


**Figure 7.** Tetrahedral decomposition of the equilibrium coexistence state whose corresponding atomic configuration is shown in Figure 5a. Dark tetrahedral faces correspond to the solid-vapor interface, while the light faces correspond to interfaces involving the liquid. On the left both solid and liquid tetrahedra are shown, while on the right only the solid tetrahedral faces are included. Note the very close correspondence between the representation given by the tetrahedral decomposition and the atomic configuration shown in Figure 5a.

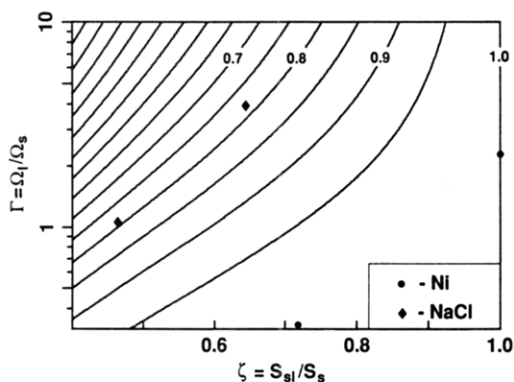


**Figure 8.** Section of the  $\Gamma$  vs  $\zeta$  plot (see Figure 3) with the results of the molecular dynamics simulations, analyzed in light of our model, included. Results for the  $(\text{NaCl})_{1000}$  cluster are denoted by a filled diamond symbol and those for the  $\text{Ni}_{1289}$  cluster by filled circles. The numbers on the contour lines correspond to values of the parameter  $\Sigma$ .

of such geometries of coexistence states ranging from two touching spheres at the nonwetting limit to a solid inclusion surrounded by a liquid at the complete wetting limit. Between these two limits partially wetted geometries occur (see schematics in Figure 1).

The molecular dynamics simulations which we performed for  $(\text{NaCl})_{1000}$  and  $\text{Ni}_{1289}$  clusters exhibit the existence and dependencies of solid-liquid equilibrium coexistence states on materials' characteristics (nature of bonding and consequently interfacial energies) and on the conditions of the cluster (energy content and thus fraction of the cluster which is molten). The results of our simulations analyzed in light of our CWM, using a modified Delaunay triangulation method (see section III.B), support the predictions of the model (see section IV). In particular, for the ionic  $(\text{NaCl})_{1000}$  cluster, we observed formation of partial wetting coexistence geometries (e.g., a liquid droplet wetting predominantly a (100) face of the solid phase; see (Figure 5a), characteristic of materials with a smaller self-wetting propensity. On the other hand, for the metallic  $\text{Ni}_{1289}$  cluster we observed formation of coexistence states where the liquid spreads over the entire surface of the faceted solid phase (see Figure 6b), characteristic of self-wetting materials (the solid-liquid interface is established preferentially on (111) facets). For both materials we found "solid lensing" configurations, where isolated (or almost isolated) facets of a solid phase otherwise covered by liquid are exposed to the vapor. In the case of NaCl, both systems exhibited

this behavior even though one had a liquid volume much greater than its solid volume ( $\Gamma \approx 4$ ; see Figure 5b). For Ni, on the other hand, this behavior was seen only in the system with an insufficient number of liquid atoms to completely cover the solid surface (see Figure 6a).

While the results of our simulations support the trends predicted by the CWM, and are also in correspondence with experimental data pertaining to the smaller self-wetting propensity of ionic materials compared to that of metals, several extensions of our model are suggested. Such possible extensions, some of which have already been performed,<sup>9,10</sup> include consideration of shape changes, crystalline anisotropies of interfacial energies, and curvature and capillary effects. We also note<sup>10</sup> that applications of such models to analyses of specific materials require reliable input data, such as crystallographic-dependent surface free energies and their temperature dependences, which are not available with sufficient accuracy for many materials. Consequently, further accurate experimental and theoretical determinations of these materials-dependent quantities are needed.

**Acknowledgment.** This research was supported by a grant from the U.S. Department of Energy (Grant No. AG05-86ER45234) and by the AFOSR. Computations were performed on CRAY computers at the National Energy Research Supercomputer Center, Livermore, California.

## References and Notes

- (1) Rose, J. P.; Berry, R. S. *J. Chem. Phys.* **1993**, *98*, 3246 and references therein.
- (2) (a) Cheng, H. P.; Berry, R. S. *Phys. Rev. A* **1992**, *45*, 7969. (b) Cheng, H. P.; Li, X.; Whetten, R. L.; Berry, R. S. *Phys. Rev. A* **1992**, *46*, 791.
- (3) Berry, R. S. *Int. J. Mod. Phys. B* **1992**, *6*, 3695.
- (4) Luo, J.; Landman, U.; Jortner, J. In *Physics and Chemistry of Small Clusters*; Jena, P., Rao, B. K., Khanna, S., Eds.; NATO ASI Series B; Plenum: New York, 1987; Vol. 158, p 155. Luo, J. Ph.D. Thesis, Georgia Institute of Technology, 1987.
- (5) Landman, U. In *Recent Developments in Computer Simulation Studies in Condensed Matter Physics*; Landau, D. P., Mon, K. K., Schuttler, H. B., Eds.; Springer: Berlin, 1988; p 108.
- (6) Nagaev, E. L. *Phys. Rep.* **1992**, *222*, 199.
- (7) Rottman, C.; Wortis, M. *Phys. Rep.* **1984**, *103*, 59.
- (8) Heyraud, J. C.; Metois, J. J.; Bermond, J. M. *J. Cryst. Growth* **1989**, *98*, 355.
- (9) Nozieres, P. *J. Phys. Fr.* **1989**, *50*, 2541.
- (10) Lowen, H. *Surf. Sci.* **1990**, *234*, 315.
- (11) Pavlovskaya, A.; Fouliau, K.; Bauer, E. *Surf. Sci.* **1989**, *221*, 233.

- (12) Ajayan, P. M.; Marks, L. D. *Phase Trans.* **1990**, 24–26, 229; *Phys. Rev. Lett.* **1988**, 60, 585; **1989**, 63, 279.
- (13) For a review of electron microscopy of small supported clusters see: Iijima, S. *Microclusters*; Springer: Berlin, 1987; p 186. Bovin, J.; Wallenberg, R.; Smith, D. *Nature* **1985**, 47, 317.
- (14) Gibbs, J. W. *Collected Works*; Longmans Green: New York, 1928.
- (15) Croxton, C. A. *Statistical Mechanics of the Liquid Surface*; Wiley: Chichester, U.K., 1980.
- (16) Rowlinson, J. S.; Widom, B. *Molecular Theory of Capilarity*; Clarendon Press: Oxford, 1982, p 38.
- (17) Wulff, G. Z. *Kristallogr. Mineral.* **1901**, 34, 449.
- (18) Herring, C. *Phys. Rev.* **1951**, 82, 87.
- (19) Cleveland, C.; Landman, U. *J. Chem. Phys.* **1991**, 94, 7376. In this paper a generalized Wulff construction formulated by L. D. Marks (*J. Cryst. Growth* **1983**, 61, 556) was applied in investigations of the structures of nickel clusters for a broad range of sizes.
- (20) Adamson, A. W. *Physical Chemistry of Surfaces*; Wiley: New York, 1976; Chapter XI.
- (21) In ref 9 (see also ref 10), the term liquid "lens" is used, in the context of a study of melting of a crystal, to describe a liquid region between two dry solid facets. In our terminology a solid "lens" is a solid region exposing a solid-vapor interface and surrounded by a liquid. A particular coexistence state may contain no solid lenses (as in the case of a solid inclusion wetted completely by a liquid). We reserve the use of the term "lensing topologies" to cases where most of the surface of the solid phase is wetted.
- (22) Daw, M. S.; Baskes, M. I. *Phys. Rev. B* **1984**, 29, 6443. Foiles, S. M.; Baskes, M. I.; Daw, M. S. *Phys. Rev. B* **1986**, 33, 7983. The parametrization which we use is that by: Adams, J. B.; Foiles, S. M.; Wolfer, W. G. *J. Mater. Res.* **1989**, 4, 102.
- (23) Chen, E. T.; Barnett, R. N.; Landman, U. *Phys. Rev. B* **1989**, 40, 924; *Phys. Rev. B* **1990**, 41, 439.
- (24) Catlow, C. R. A.; Diller, K. M.; Norgett, M. J. *J. Phys. C* **1977**, 10, 1395. In our calculations the effective second-neighbor  $1/r^6$  term was neglected.
- (25) Allen, M. P.; Tildesley, D. J. *Computer Simulations of Liquids*; Clarendon: Oxford, 1987.
- (26) Abraham, F. F. *J. Chem. Phys.* **1978**, 68, 713.
- (27) Landman, U.; Brown, C. S.; Cleveland, C. L. *Phys. Rev. Lett.* **1980**, 45, 2032. See also: *Nonlinear Phenomena at Phase Transitions and Instabilities*; Riste, T., Ed.; Plenum: New York, 1981; p 379.
- (28) Barnett, R. N.; Landman, U.; Cleveland, C. L.; Rast, R. H. *J. Vac. Sci. Technol.* **1985**, 3, 1574.
- (29) Landman, U.; Luedtke, W. D.; Ribarsky, M. W.; Cleveland, C. L.; Barnett, R. N. *Phys. Rev. B* **1988**, 37, 4637.
- (30) Barnett, R. N.; Landman, U. *Phys. Rev. B* **1991**, 44, 3226.
- (31) Van der Veen, J. F.; Pluis, B.; Denier Van der Gon, A. W. In *Kinetics of Ordering at Surfaces*; Lagally, M. G., Ed.; Plenum: New York, 1990; p 343.
- (32) Dividing the standard deviation by the square root of the length of time interval results in a quantity that is relatively insensitive to that length.
- (33) Bowyer, A. *Comput. J.* **1981**, 24, 162. Watson, D. F. *Comput. J.* **1981**, 24, 167. Avis, D.; Bhattacharya, B. K. In *Advance in Computing Research I*; Preparata, F. P., Ed.; JAI Press: New York, 1983. Barry Joe, *Comput.-Aided Geom. Des.* **1991**, 8, 123. Dey, T. K.; Sugihara, K.; Bajaj, C. L. *Comput.-Aided Geom. Des.* **1992**, 9, 457; among others.
- (34) GEOMPACK, developed by Barry Joe, may be obtained by anonymous ftp to menaik.cs.ualberta.edu. or by e-mail request to barry@cs.ualberta.edu.
- (35) To estimate values of  $\Sigma \equiv (\sigma_{sv} - \sigma_{sl})/\sigma_{lv}$ , we searched the literature for measured and calculated values of the interfacial energies of sodium chloride and nickel. For NaCl, with values given by E. R. Buckle and A. R. Ubbelohde (*Proc. R. Soc. London A* **1961**, 261, 197, we obtain  $\Sigma(\text{NaCl}) \approx 0.8$ , which agrees with the results of our simulations and the prediction of the CWM shown in Figure 8. (We remark that using other published values for the interfacial energies yields  $0.65 \lesssim \Sigma(\text{NaCl}) \lesssim 0.8$ ). For nickel, using experimental values  $\sigma_{sv} = 1920 \text{ erg/cm}^2$  (at 1627 K; see: Wawra, H. Z. *Metallk.* **1975**, 66, 395, citing Bryant, L. F.; Splisoe, R.; Hirth, J. P. *Trans. AIME* **1968**, 242, 1145),  $\sigma_{sl} = 255 \text{ erg/cm}^2$  (after Turnbull, D. *J. Appl. Phys.* **1950**, 21, 1022), and  $\sigma_{lv} = 1733 \text{ erg/cm}^2$  (at the melting point, 1728 K; see *Handbook of Chemistry and Physics*, 55th ed. CRC: Cleveland, 1974), we obtain  $\Sigma(\text{Ni}) = 0.96$  (using other experimental values yields values  $\geq 1$ ). This estimate is also in agreement with our results shown in Figure 8, reflecting the higher self-wetting propensity of nickel compared to that of sodium chloride.